

See discussions, stats, and author profiles for this publication at: <https://www.researchgate.net/publication/215715177>

Reversible Tunability of the NIR Valence Band Plasmon Resonance in Cu_{2-x}Se Nanocrystals.

ARTICLE · JANUARY 2011

READS

146

9 AUTHORS, INCLUDING:



Nadja C Bigall

Leibniz Universität Hannover

49 PUBLICATIONS 1,180 CITATIONS

[SEE PROFILE](#)



Alessandro Genovese

King Abdullah University of Science and Tec...

61 PUBLICATIONS 1,377 CITATIONS

[SEE PROFILE](#)



Liberato Manna

Istituto Italiano di Tecnologia

316 PUBLICATIONS 16,199 CITATIONS

[SEE PROFILE](#)

Reversible Tunability of the Near-Infrared Valence Band Plasmon Resonance in Cu_{2-x}Se Nanocrystals

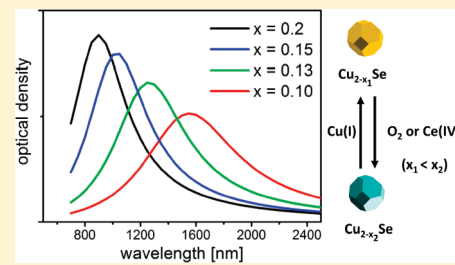
Dirk Dorfs,[†] Thomas Härtling,[‡] Karol Miszta,[†] Nadja C. Bigall,[†] Mee Rahn Kim,[†] Alessandro Genovese,[†] Andrea Falqui,[†] Mauro Povia,[†] and Liberato Manna^{*†}

[†]Istituto Italiano di Tecnologia, Via Morego 30, 16163 Genova, Italy

[‡]Fraunhofer Institute for Non-Destructive Testing, Dresden Branch, Maria-Reiche-Strasse 2, 01109 Dresden, Germany

Supporting Information

ABSTRACT: We demonstrate that colloidal Cu_{2-x}Se nanocrystals exhibit a well-defined infrared absorption band due to the excitation of positive charge carrier oscillations (i.e., a valence band plasmon mode), which can be tuned reversibly in width and position by varying the copper stoichiometry. The value of x could be incrementally varied from 0 (no plasmon absorption, then a broad peak at 1700 nm) to 0.4 (narrow plasmon band at 1100 nm) by oxidizing Cu_2Se nanocrystals (upon exposure either to oxygen or to a Ce(IV) complex), and it could be incrementally restored back to zero by the addition of a Cu(I) complex. The experimentally observed plasmonic behavior is in good agreement with calculations based on the electrostatic approximation.



1. INTRODUCTION

Achieving fine-tunability in the optical properties of colloidal nanocrystals is one of the main focuses of research in nanoscience, ever since the new field of wet chemical synthesis of these types of materials has emerged. The two major classes of nanoparticles with tunable optical absorption behavior are semiconductor^{1–5} and metal nanocrystals.^{6–9} In semiconductor nanocrystals, the absorption properties can be finely varied by adjusting the particle radius, when this is smaller than the Bohr exciton radius of the corresponding bulk material. In metal nanoparticles, the plasmonic response is strongly dependent on the type of metal of which they are made, on the dielectric function of the surrounding medium, as well as on the particle shape and to a lesser extent on the nanoparticle size. The optical absorption properties of semiconductor nanocrystals remain practically fixed at the end of their synthesis and can be altered only slightly by post synthetic treatments (barring chemical treatments that can alter their size and/or shape), while in metallic nanoparticles the spectral position of the plasmon peaks can be still strongly affected by the surrounding medium.^{6–9} On the other hand, while many types of semiconductor nanoparticles are available such that the whole region of the optical spectrum from deep ultraviolet (UV) to several micrometers in the infrared (IR) can be covered (depending on the target application), only a handful of metals are available, which show useful plasmonic properties; among them, the most exploited are Ag, Au, Cu, and Pt,^{10–14} and these are mainly in the visible range and in the UV. Furthermore, systematic investigations of the IR response were reported only for Au-based nanostructures.^{15–18}

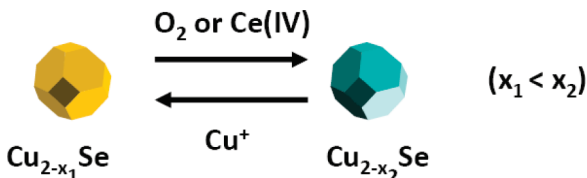
Also, a considerable effort has been put in the last years into the synthesis of Cd-free semiconductor nanocrystals. Among them, Cu_2Se and Cu_2S nanocrystals are promising, as they have

direct band gaps in the range of their Cd analogues (1.2 eV for bulk Cu_2S and 2.2 eV for bulk Cu_2Se), and many studies on the synthesis of nanocrystals of these materials and on their physical properties have appeared.^{19–23} It is also known that copper in them can exist in a wide range of stoichiometries in addition to the 2:1 one with respect to Se and S, and its influence on the optical response in the infrared region has been a subject of interest in the past decade. A recent work by Burda et al. on Cu_{2-x}S nanocrystals interpreted the strong NIR absorption in these nanoparticles as plasmonic in origin,²¹ a valence band plasmon absorption, due to the high density of holes when x in Cu_{2-x}S is greater than zero, which also explains the absence of the strong NIR band in both stoichiometric (or nearly stoichiometric) Cu_2S and Cu_2Se nanocrystals.²¹ The work gave a qualitative interpretation of the observed NIR absorption and was based on Cu_{2-x}S nanocrystals with three distinct values of x . Early this year, while the present work was under review, Alivisatos et al. reported a detailed study on plasmonic properties of Cu_{2-x}S nanocrystals, which showed how starting from nearly stoichiometric Cu_2S particles, their oxidation (upon exposure to air) increased the degree of copper deficiency and led to the emergence of an IR band that gradually increased in intensity and slightly blue-shifted in energy.²⁴ The behavior was correlated to a plasmonic effect due the creation of holes in the valence band of Cu_{2-x}S , and the study was supported by calculations. Also, Cu_{2-x}Se nanocrystals show an intense and well-defined NIR absorption band in addition to the visible absorption band, the latter due to the direct band gap transition. Various groups, including ours in an earlier work on the synthesis of Cu_{2-x}Se

Received: February 21, 2011

Published: July 06, 2011

Scheme 1. Reversible Oxidation/Reduction of Cu_{2-x}Se Nanocrystals^a



^a Oxidation, which increases copper deficiency, could be carried out either by exposure to air or by stepwise addition of a Ce(VI) complex. Reduction, which decreases copper deficiency, could be carried out by addition of a Cu(I) complex.

nano-crystals,¹⁹ adopted the explanation that this absorption corresponds to a transition belonging to an indirect band gap of Cu_{2-x}Se , at least for x around 0.2.²⁵ Previous reports by Yumashev et al. and Gurin et al. on glasses containing oxidized Cu_2Se nanoparticles assigned instead the IR band to a “photodarkening effect”, to transitions involving electrons trapped in long-lived deep trap states in the glass matrix.^{26,27} However, enough evidence so far has been brought, most notably by Burda’s and Alivisatos’ works on Cu_{2-x}S nanoparticles discussed above,^{21,24} that also in Cu_{2-x}Se this peak should be assigned to a plasmon resonance. Indeed, a recent work by Korgel et al. on Cu_{2-x}Se nanoparticles (while the present work was under review) made such a statement and furthermore demonstrated that the NIR band could be exploited for photothermal therapy applications.²⁸

Here, we report the reversible tuning of the near-infrared plasmonic response of colloidal Cu_{2-x}Se nanocrystals (synthesized according to a procedure reported by us in a previous work¹⁹) via a post synthetic, gradual oxidation of Cu_{2-x}Se nanocrystals, either under ambient conditions (i.e., under air) or by stepwise addition of a Ce(IV) complex. The oxidation process was responsible for the decrease of the Cu:Se stoichiometry from values close to 2:1 of the nanocrystals “as-synthesized” down to the lower limit of 1.6:1; that is, “ x ” could be varied from 0 to 0.4 (for Ce^{4+} -based oxidation, Scheme 1). The stoichiometry for these two extreme compositions was assessed via in situ elemental analysis in the transmission electron microscope (TEM); see below. During this variation in x , the optical response in the near-infrared region evolved from a broad band around 1700 nm ($\text{Cu}_{1.96}\text{Se}$),²⁹ to a symmetric and narrower band shifted at shorter wavelengths, down to a narrow band at 1100–1150 nm for the most oxidized species. A subsequent, gradual reduction of the resulting copper deficient nanocrystals by the addition of Cu^+ ions could restore the optical response of the “as-synthesized” samples; that is, x could be again decreased. Further addition of Cu(I) salt led to disappearance of the absorption band (hence to a reduction of x to 0).²⁹ However, controlled oxidation could restore the absorption in the IR. Hence, by means of the two reversible oxidation and reduction processes, a control over x in the range from 0 to 0.2 (for oxidation with O_2) or from 0 to 0.4 (for oxidation with Ce^{4+}) could be achieved, which allowed to continuously fine-tune the NIR absorption band of these nanocrystals in the 1100–1700 nm range. These studies were supported by computations in the framework of the electrostatic approximation for a conductive nanosphere interacting with an external electric field.

Overall, the present study demonstrates how the IR plasmonic behavior of such Cu_{2-x}Se nanoparticles can be tuned reversibly

on the basis of their copper deficiency, which can be increased by various oxidation means (we report here the oxidation under air and by a Ce(IV) complex) or decreased by the addition of a Cu(I) complex.

2. EXPERIMENTAL SECTION

Chemicals. Copper chloride (CuCl, 99.999%) and elemental selenium (Se, 99.99%) were purchased from Strem chemicals. Tetrakis(acetonitrile)-copper(I) hexafluorophosphate, oleylamine (OLAM, 70%), oleic acid (OLAC, 90%), 1-octadecene (ODE, 90%), tetrachloroethylene (spectroscopic grade), and 1-butanol were purchased from Sigma-Aldrich. Anhydrous ethanol, toluene, and chloroform, as well as cerium(IV)–ammonium nitrate (>98.5%) were purchased from Carlo Erba reagents. All chemicals were used without further purification.

Synthesis of Cu_{2-x}Se Nanoparticles. The synthesis of Cu_{2-x}Se particles was a slightly adapted variation of the one previously published by us:¹⁹ Anhydrous CuCl (0.09 g, 1 mmol) was first added to a mixture of 5 mL of oleylamine and 5 mL of 1-octadecene (ODE) in a reaction flask. After evacuation for 1 h at 80 °C using standard Schlenk line technique, the reaction mixture was exposed to a constant flow of nitrogen. The temperature was then set to 300 °C. A solution of Se in oleylamine was freshly prepared by mixing 0.039 g of Se (0.5 mmol) with 3 mL of oleylamine. Subsequently, the oleylamine/selenium mixture was heated to 150 °C under vacuum for 1 h using standard Schlenk line technique followed by switching to a nitrogen flow and heating to 230 °C for 1 h to fully dissolve the selenium. This solution was then cooled to 100 °C. The solution was kept at this temperature and transferred into a glass syringe equipped with a large needle (12 gauge external diameter) and injected quickly into the flask. After the injection, the temperature of the reaction mixture dropped to 280 °C, and it was allowed to recover to the preinjection value. The overall reaction time after injection was 15 min, after which the flask was rapidly cooled to room temperature. Once at room temperature, 5 mL of toluene was added to the reaction mixture, the resulting solution was transferred into a vial under a blanket of nitrogen, and the vial was then stored inside a glovebox. This solution was then washed by precipitation (via addition of ethanol) and redissolution in toluene. After the washing step, the Cu_{2-x}Se nanocrystals were dissolved in 3 mL of toluene.

Optical Spectroscopy. For acquiring the extinction spectra, the particles dissolved in toluene were dried in a flow of nitrogen followed by redispersion in tetrachloroethylene or toluene. These solutions were measured in a 1 cm quartz cuvette using a Varian Cary 5000 UV-vis-NIR absorption spectrophotometer. Under inert gas conditions, airtight screw cap cuvettes were used.

Oxidation of the Cu_{2-x}Se Nanocrystals under Ambient Conditions. The original Cu_{2-x}Se nanoparticles stored in an inert atmosphere glovebox were taken out of the glovebox and oxidized under ambient conditions. In toluene, the oxidation process lasted for around 24 h, while in tetrachloroethylene the same oxidation occurred within 1 h.

Oxidation of the Cu_{2-x}Se Nanocrystals under Oxygen-Free Conditions. The Cu_{2-x}Se nanoparticles were oxidized by adding small volumes of $\text{NH}_4\text{Ce}(\text{NO}_3)_6$ dissolved in butanol or ethanol (0.1 M solution in ethanol or 0.05 M solution in butanol) under oxygen-free conditions in an inert atmosphere glovebox.

Reduction of Cu_{2-x}Se Nanocrystals by Addition of Cu(I) Salt. 37 mg of $\text{Cu}(\text{I})(\text{CH}_3\text{CN})_4\text{PF}_6$ was dissolved in 5 mL of methanol resulting in a 0.02 M solution. This solution was added in portions of 5 μL directly into the cuvette containing the Cu_{2-x}Se nanoparticles, and the absorption spectra were recorded immediately afterward.

Transmission Electron Microscopy and STEM Analysis. High-resolution TEM (HRTEM), high angular annular dark field (HAADF), scanning TEM (STEM), and energy filtered TEM (EFTEM)

measurements were performed with a JEOL JEM-2200FS microscope, equipped with a field emission gun working at an accelerating voltage of 200 kV, a CEOS spherical aberration corrector of the objective allowing to reach a spatial resolution of 0.9 Å, and an in column Omega filter. Single particle chemical composition was determined for several particles by energy dispersive X-ray spectroscopy (EDS) analysis performed in STEM mode, with a JED-2300 Si(Li) detector and an electron probe size of 0.7 Å. EFTEM images were acquired using a contrast aperture of about 10 mrad to reduce aberrations (mostly chromatic). The elastic image (or zero-loss image) was acquired as reference with a 10 eV wide energy slit. Chemical maps using the O K-edge (532 eV), Cu L-edge (931 eV), and Se L-edge (1436 eV) were acquired on the same area with an energy slit of 30, 50, and 60 eV, respectively.

Calculations of the Nanoparticle Extinction Spectra. The extinction spectra of the Cu_{2-x}Se nanocrystals were calculated for the spectral region between 700 and 2500 nm as described in the following. The computation was carried out using the electrostatic approximation for the interaction of a conductive nanosphere with an external electric field.³⁰ No significant retardation of the electromagnetic field over the particle occurs for the radius-to-wavelength ratio studied here, and therefore the electrostatic approximation is justified. The extinction cross section σ_{ext} is given by $\sigma_{\text{ext}} = \sigma_{\text{abs}} + \sigma_{\text{sca}}$, with σ_{abs} as the absorption cross section and σ_{sca} as the scattering cross section. Within the electrostatic approximation for spherical particles, these values, for the dipolar mode, are given by

$$\sigma_{\text{abs}} = k \cdot \text{Im} \left[4\pi r^3 \frac{\varepsilon(\omega) - \varepsilon_m}{\varepsilon(\omega) + 2\varepsilon_m} \right] \quad (1)$$

$$\sigma_{\text{sca}} = \frac{8}{3} \pi k^4 r^6 \left| \frac{\varepsilon(\omega) - \varepsilon_m}{\varepsilon(\omega) + 2\varepsilon_m} \right|^2 \quad (2)$$

with k being the wave vector of the incident light, r the particle radius, $\varepsilon(\omega)$ the dielectric function of the particle material, and ε_m the dielectric constant of the surrounding medium. Tetrachloroethylene with a refractive index of $n = 1.505$ was used as surrounding medium. Therefore, $\varepsilon_m = n^2$ amounts to 2.25. The dielectric function $\varepsilon(\omega) = \varepsilon_1(\omega) + i\varepsilon_2(\omega)$ for different values of x ($x = 0.1, 0.13, 0.15$, and 0.2) was calculated from bulk reflectivity measurement data reported in ref 31. The respective real $\varepsilon_1(\omega)$ and imaginary $\varepsilon_2(\omega)$ parts are given by

$$\varepsilon_1(\omega) = n^2 - k^2 = \varepsilon_\infty - 4\pi e^2 \frac{p}{m^*} \left(\frac{\langle \tau \rangle^2}{1 + \omega^2 \langle \tau \rangle^2} \right) \quad (3)$$

and by

$$\varepsilon_2(\omega) = 2nk = \varepsilon_0 - 4\pi e^2 \frac{p}{\omega m^*} \left(\frac{\langle \tau \rangle}{1 + \omega^2 \langle \tau \rangle^2} \right) \quad (4)$$

These equations contain the following parameters: p is charge carrier concentration, τ is carrier relaxation time, m^* is effective mass of the charge carrier, e is elementary charge, ε_0 is vacuum permittivity, ε_∞ is high-frequency dielectric constant, and ω is light frequency. The computed real and imaginary parts of the dielectric functions for various Cu_{2-x}Se stoichiometries are reported in the Supporting Information. The use of the bulk data for the dielectric function of the particles is possible because for the particle diameter of 15 nm the dielectric function does not yet show any size dependence.³²

3. RESULTS AND DISCUSSION

The trend in optical properties observed by us on Cu_{2-x}Se nanocrystals upon oxidation under air is displayed in Figure 1a. Upon gradual oxidation, the optical response in the near-infrared

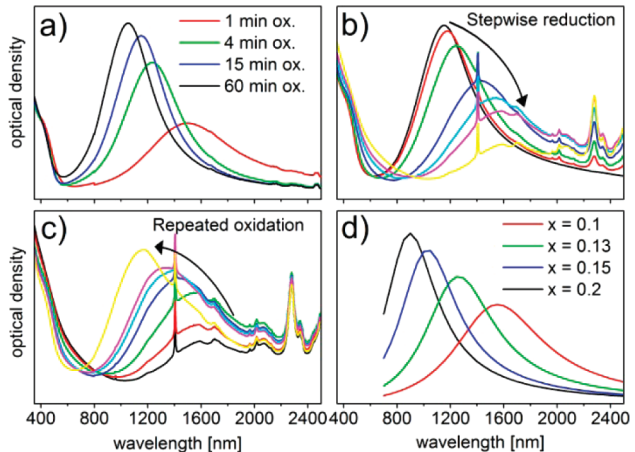


Figure 1. (a) Evolution of the extinction spectrum of the “as-synthesized” $\text{Cu}_{1.96}\text{Se}$ nanocrystals (dissolved in tetrachloroethylene) over time, when they are gradually oxidized, under ambient conditions, to $\text{Cu}_{1.81}\text{Se}$ (as found by elemental analysis). (b) Evolution of the extinction spectra of the oxidized sample ($\text{Cu}_{1.81}\text{Se}$) when treated with different amounts of a Cu(I) salt. Each step from the black toward the yellow spectrum corresponds to an addition of 5 μL of a 0.02 M $\text{Cu}(\text{CH}_3\text{CN})_4\text{PF}_6$ solution. (c) Evolution of the extinction spectra of the reduced sample from (b) when again oxidized under ambient conditions for 19 h in total from the black to the yellow spectrum. The sharp absorption peaks in panels (b) and (c) are due to absorption of methanol and the Cu(I) salt. (d) Calculated extinction spectra of single Cu_{2-x}Se nanocrystals for different x values.

region evolved from a broad band around 1700 nm to the emergence of a symmetric and slightly narrower band at 1500 nm, then to a gradual spectral shift and narrowing, down to a narrow band at 1100–1150 nm. To gain further insight into the IR optical properties of the Cu_{2-x}Se nanocrystals, we calculated their optical extinction spectra using the electrostatic approximation for the interaction of a dielectric nanosphere with an external electric field, as described above.^{30,33} The calculated spectra (Figure 1d)²⁹ for Cu_{2-x}Se particles with different degrees of copper deficiency (i.e., “ x ”) evidenced a blue shift for larger x , a narrowing of the plasmon extinction band, and a higher oscillator strength with increasing x . All of these trends are in line with our experimental findings, because via elemental quantification by EDS in the TEM we found that oxidation indeed causes a chemical transformation from Cu_{2-x}Se with $x < 0.1$ to Cu_{2-x}Se with x close to 0.2 (see below). A similar chemical transformation was observed by Riha et al. starting from Cu_2Se nanocrystals,²³ and the increase in conductivity in films of initial Cu_2Se nanoparticles was ascribed to a combination of effects, among them also the formation of p-type conducting Cu_{2-x}Se . Comparison of our experiments and calculations therefore allows us to assign the infrared absorption to a dipole plasmon excitation rather than to a transition belonging to an indirect band gap, in good agreement with the latest findings of Alivisatos et al. on Cu_{2-x}S nanoparticles.²⁴

The time frame of the oxidation procedure under ambient conditions shown in Figure 1a is not very well controllable at present, as the oxidation rate depends on many parameters, such as the type of solvent and the rate of dissolution of oxygen in the solvent (which in turn depends on various parameters). Indeed, a better control over the value of x in Cu_{2-x}Se nanocrystals can be achieved via the post synthetic reduction procedure where we

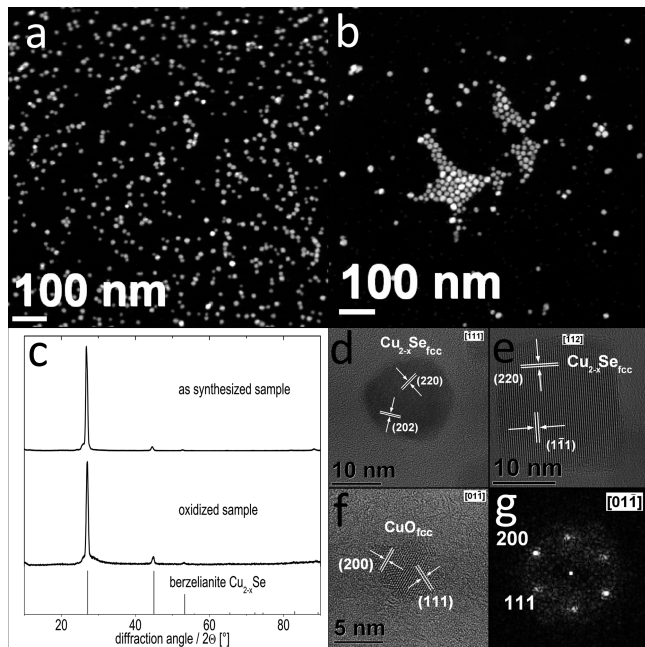


Figure 2. (a,b) HAADF-STEM survey images of the “as-synthesized” unoxidized Cu_{2-x}Se nanocrystals (a) and of the oxidized Cu_{2-x}Se nanocrystals (b). (c) X-ray diffraction of the “as-synthesized” sample and of the oxidized one, along with the bulk reflexes of berzelianite Cu_{2-x}Se . (d,e) HRTEM images of a nanocrystal belonging to the “as-synthesized” sample (d) and of a nanocrystal belonging to the oxidized sample (e). (f,g) HRTEM image and corresponding numerical diffractogram (i.e., the filtered 2D-FFT) of a small CuO particle present in the oxidized sample.

start from oxidized Cu_{2-x}Se nanoparticles and then add small amounts of Cu^+ ions, as reported in Figure 1b. This reduction reaction is practically instantaneous for the time scale of the measurements and allows a precise control over the value of x and hence the position of the plasmonic absorption between 1100 and 1700 nm for the solvent used (Figure 1b). Here, we see again a very well-defined red shift of the plasmon absorption with each subsequent addition of Cu(I) . Also, in this case, the comparison to our calculations indicates a change in x from around $x = 0.2$ to a value of $x < 0.1$ (for smaller values of x no modeling was possible, due to missing literature data of the physical properties of the bulk material in this case). Furthermore, the same sample of nanocrystals could be oxidized again; hence the process observed in Figure 1a and b is reversible (Figure 1c).

X-ray diffraction (XRD) data indicated that the crystal structures of the pristine (reduced) particles and of the oxidized ones were both cubic berzelianite Cu_{2-x}Se (Figure 2c). This is in good agreement with the assumption that the oxidation creates cation vacancies in the lattice without altering the actual structure of the nanocrystal. These cation vacancies lead to the formation of holes in the valence band of the nanocrystals, while the band structure itself remains practically unperturbed, as the crystal symmetry does not change. As a result, the charge carriers in the valence band become mobile, which leads to p-type conductivity^{19,23} and to the possibility to excite valence band plasmons. The number of mobile carriers created is significant. As an example, a nanocrystal with a diameter of 15 nm, initially made of stoichiometric berzelianite Cu_2Se , contains around 1.2×10^5 atoms (after weighing the various Cu occupancies in the lattice), of which around 8×10^4 atoms are Cu . Even removing

5% of the total Cu atoms, so as to yield $\text{Cu}_{1.90}\text{Se}$, means expelling 4×10^3 Cu atoms from a single nanocrystal.

Survey HAADF-STEM images (Figure 2a,b) of nanocrystal samples before and after oxidation indicated that the size and shape distribution of the Cu_{2-x}Se nanocrystals remained unchanged upon oxidation under ambient conditions, but some new (small) nanoparticles were formed. Energy filtered imaging in the TEM (EFTEM) revealed that these small nanoparticles contain Cu and O .²⁹ They were actually made of CuO , as clearly assessed via HRTEM on some of the very few particles that were 4–5 nm in size, for which the filtered 2D-FFT image could be indexed reliably (Figure 2f,g). These nanocrystals were not present in the pristine sample, so they were formed via reaction of oxygen with the copper species expelled from the Cu_{2-x}Se nanocrystals. Because these nanocrystals were much smaller than the Cu_{2-x}Se ones and they were present as a small fraction, they practically did not contribute to the overall X-ray diffraction of the ensemble. EFTEM of all of the big nanocrystals instead indicated that they were formed by Cu and Se , with a faint halo of oxygen, most likely due to the presence of a thin surface copper oxide layer.²⁹ Quantitative analysis on these big particles, carried out via EDS on several nanocrystals for each sample, yielded a weighted $\text{Cu}:\text{Se}$ ratio equal to 1.96 for the pristine Cu_{2-x}Se sample, and 1.81 for the oxidized one.²⁹ HRTEM confirmed that in both samples the Cu_{2-x}Se nanocrystals had cubic berzelianite phase (Figure 2d,e). Summarizing the data from structural characterization, we can conclude that the structural changes to the Cu_{2-x}Se nanocrystals are minor during the oxidation process by oxygen and that the Cu^{2+} species created during oxidation, which are “ejected” from the nanocrystals, form separate, small CuO nanocrystals. Nonetheless, the small stoichiometric variation in the Cu_{2-x}Se nanocrystals is responsible for the large differences in NIR absorption behavior observed by us.

We consider it unlikely that the plasmonic behavior found here was due to the formation of a copper oxide layer (most likely CuO) around the nanocrystals. First, the dielectric function of this material indicates unambiguously that in CuO the electrostatic plasmon resonance condition is never fulfilled in the region of interest (i.e., between 700 and 2500 nm).²⁹ Also, a thick copper oxide layer around the nanoparticles would most likely prevent the restoration of the $\text{Cu}:\text{Se}$ stoichiometry upon addition of the Cu(I) species, which is contrary to our observation. Other possibilities for the thin oxide layer to influence the plasmonic response are: (i) a dielectric effect, which however would shift the plasmon resonance to longer wavelengths, thus in an opposite direction from what we observe; and (ii) a charge transfer effect. CuO is a p-type conductive material; hence it could inject additional holes in the Cu_{2-x}Se “core”, thereby increasing the hole density and shifting the resonance frequency to lower wavelengths.

One experiment that safely ruled out a major contribution of this CuO layer to the plasmonic behavior of the nanocrystals, and actually the most convincing proof that the plasmonic behavior is indeed due to the substoichiometric composition of copper, was provided by a set of oxidation experiments carried out under inert atmosphere and using a Ce(IV) complex as oxidizing agent, by adding a solution of $\text{NH}_4\text{Ce}(\text{NO}_3)_6$ in anhydrous butanol to a solution of Cu_{2-x}Se nanocrystals, hence in the absence of oxygen. We actually found this procedure to be more controllable than the previous one involving oxygen, which is not precisely tunable as the oxygen dissolution depends on too many (and not well controlled) parameters. The redox potential of Ce^{4+} is even slightly more positive than the one of oxygen, so that

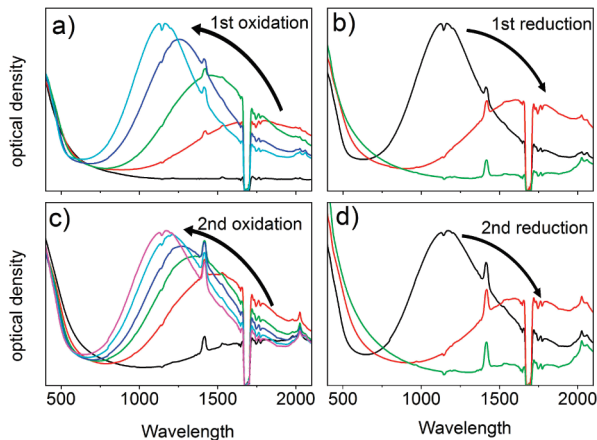


Figure 3. Extinction spectra corresponding to two cycles of oxidation and reduction of the same sample using stepwise Ce^{4+} addition for oxidation and Cu^+ addition for reduction. (a) Each step from the black to the light blue spectrum corresponds to an addition of 5 μL of a 0.1 M solution of $\text{NH}_4\text{Ce}(\text{NO}_3)_6$ in ethanol. (b) Each step from the black to the green spectrum corresponds to an addition of 5 μL of a 0.1 M solution of $\text{Cu}(\text{CH}_3\text{CN})_4\text{PF}_6$ in methanol. (c) Repetition of the procedure as done in (a). (d) Repetition of the procedure as done in (b). In these experiments, the Cu_{2-x}Se nanoparticles were dissolved in toluene (which also causes the spectral feature at 1700 nm that is due to the very high optical density of toluene in this spectral region).

Ce^{4+} should surely be able to oxidize Cu^+ to Cu^{2+} . In this case, the oxidation reaction was quasi instantaneous, and it could be controlled easily via the amount of Ce^{4+} ions added to the solution of Cu_{2-x}Se nanocrystals. Again the oxidation could be reversed by addition of Cu^+ ions. Figure 3 shows the extinction spectra corresponding to two cycles of oxidation and reduction of the same sample using stepwise Ce^{4+} additions for the oxidation and Cu^+ additions for the reduction. Again, the plasmon resonance could be tuned between 1100 nm for the most oxidized sample and 1700 nm and finally no plasmon resonance for the sample with $\text{Cu}:\text{Se}$ stoichiometry close to 2:1. Upon complete reduction to Cu_2Se ($x = 0$), the plasmon absorption vanished, but could be restored by repeated addition of Ce^{4+} . Hence, using Ce^{4+} as oxidizing agent and Cu^+ as reducing agent, the plasmon absorption of the particles could be tuned reversibly and with a high degree of control.

Elemental quantification (via EDS) of single particles oxidized by means of $\text{Ce}(\text{IV})$ and exhibiting an absorption band around 1150 nm indicated a similar trend when compared to the original sample as observed in the case of O_2 -induced oxidation (x increased from a value close to 0 to a value around 0.3–0.4 in the case of cerium induced oxidation; see Figure 4 as well as the Supporting Information for more details on elemental analysis). Also, no CuO particles were found, nor any significant oxygen signal was detected from the Cu_{2-x}Se particles in this set of samples, which was somehow expected due to the absence of oxygen during the oxidation procedure.²⁹ Furthermore, no signal from Ce was detected from the particles, indicating that the $\text{Ce}(\text{IV})/\text{Ce}(\text{III})$ redox couple was not involved in any cation exchange reactions with the nanocrystals. All of these experiments clearly rule out any major influence of a copper oxide layer or any other exchange reaction on the plasmonic properties of the particles. Also, HR-TEM analysis of the oxidized and the original sample in the case of Ce^{4+} induced oxidation clearly

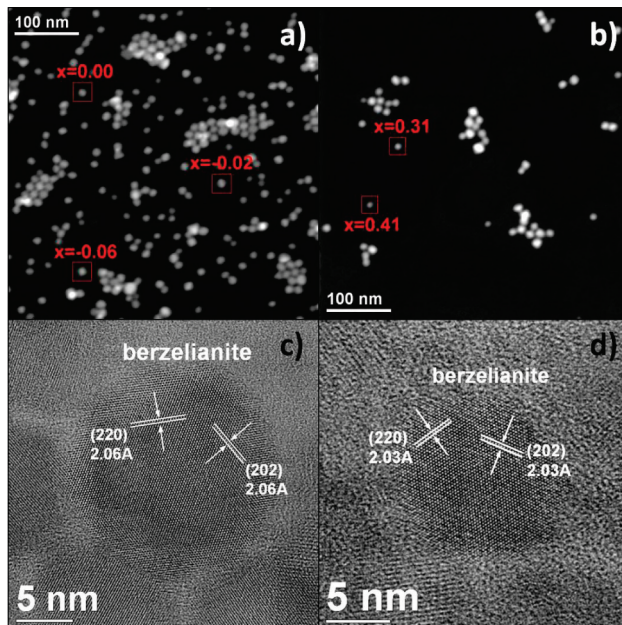


Figure 4. HAADF-STEM images of the (a) pristine and the (b) oxidized sample using Ce^{4+} for oxidation. Elemental compositions of single particles are indicated. HR-TEM images of the (c) pristine and (d) oxidized particles using Ce^{4+} oxidation indicating that the berzelianite phase is unchanged during oxidation.

shows that the Cu_{2-x}Se nanoparticles stay unchanged in the berzelianite phase during the oxidation procedure. This supports the fact that the only difference between the oxidized and the reduced samples is indeed the degree of Cu deficiency, which is in excellent agreement with our optical observations as well as our theoretical calculations.

4. CONCLUSION

We demonstrate that, by oxidation/reduction of Cu_{2-x}Se nanocrystals, we are able to modify the degree of copper deficiency in them, and consequently we are able to tune their valence band plasmon resonance, both in shape and in position, over a broad spectral range in the near-infrared spectral region. This represents a novelty with respect to the more traditional plasmonic nanoparticles not only in terms of the broad accessible wavelength regime but also due to the easy postsynthetic and reversible tunability of the plasmon resonance. In addition, these materials are more economically viable to make than are the noble metal nanoparticles. The oxidation process of the Cu_{2-x}Se nanocrystals under both ambient conditions and via addition of a $\text{Ce}(\text{IV})$ complex can be completely reversed by the addition of a $\text{Cu}(\text{I})$ complex. Calculations in the framework of the electrostatic approximation were in good agreement with the optical absorption spectra measured by us. These findings add another candidate to the class of NIR plasmonic materials, and the spectral range that is accessible by these nanoparticles is highly appealing for IR spectroscopy and imaging applications, which might also profit considerably from the benefit of the “in situ” tunable absorption of these particles.

■ ASSOCIATED CONTENT

S Supporting Information. Details on the synthesis, oxidation, and reduction processes of the nanocrystals, on electron

microscopy analysis, and on the dielectric functions used for the calculations. This material is available free of charge via the Internet at <http://pubs.acs.org>.

AUTHOR INFORMATION

Corresponding Author

liberato.manna@iit.it

ACKNOWLEDGMENT

We acknowledge financial support from European Union through the FP7 starting ERC grant NANO-ARCH (contract number 240111). Funding by FhG Internal Programs (Grant No. ATTRACT 692271) is gratefully acknowledged.

REFERENCES

- (1) El-Sayed, M. A. *Acc. Chem. Res.* **2004**, *37*, 326–333.
- (2) Eychmuller, A. *J. Phys. Chem. B* **2000**, *104*, 6514–6528.
- (3) Scholes, G. D.; Rumbles, G. *Nat. Mater.* **2006**, *5*, 683–696.
- (4) Talapin, D. V.; Lee, J. S.; Kovalenko, M. V.; Shevchenko, E. V. *Chem. Rev.* **2010**, *110*, 389–458.
- (5) Trindade, T.; O'Brien, P.; Pickett, N. L. *Chem. Mater.* **2001**, *13*, 3843–3858.
- (6) Link, S.; El-Sayed, M. A. *Int. Rev. Phys. Chem.* **2000**, *19*, 409–453.
- (7) Kelly, K. L.; Coronado, E.; Zhao, L. L.; Schatz, G. C. *J. Phys. Chem. B* **2003**, *107*, 668–677.
- (8) Noguez, C. *Opt. Mater.* **2005**, *27*, 1204–1211.
- (9) Myroshnychenko, V.; Rodriguez-Fernandez, J.; Pastoriza-Santos, I.; Funston, A. M.; Novo, C.; Mulvaney, P.; Liz-Marzan, L. M.; de Abajo, F. J. *G. Chem. Soc. Rev.* **2008**, *37*, 1792–1805.
- (10) Bastys, V.; Pastoriza-Santos, I.; Rodriguez-Gonzalez, B.; Vaisnoras, R.; Liz-Marzan, L. M. *Adv. Funct. Mater.* **2006**, *16*, 766–773.
- (11) Link, S.; Wang, Z. L.; El-Sayed, M. A. *J. Phys. Chem. B* **1999**, *103*, 3529–3533.
- (12) Klar, T.; Perner, M.; Grosse, S.; von Plessen, G.; Spirk, W.; Feldmann, J. *Phys. Rev. Lett.* **1998**, *80*, 4249–4252.
- (13) Bigall, N. C.; Hartling, T.; Klose, M.; Simon, P.; Eng, L. M.; Eychmuller, A. *Nano Lett.* **2008**, *8*, 4588–4592.
- (14) Chan, G. H.; Zhao, J.; Hicks, E. M.; Schatz, G. C.; Van Duyne, R. P. *Nano Lett.* **2007**, *7*, 1947–1952.
- (15) Bardhan, R.; Grady, N. K.; Halas, N. J. *Small* **2008**, *4*, 1716–1722.
- (16) Bardhan, R.; Grady, N. K.; Cole, J. R.; Joshi, A.; Halas, N. J. *ACS Nano* **2009**, *3*, 744–752.
- (17) Neubrech, F.; Kolb, T.; Lovrincic, R.; Fahsold, G.; Pucci, A.; Aizpurua, J.; Cornelius, T. W.; Toimil-Molares, M. E.; Neumann, R.; Karim, S. *Appl. Phys. Lett.* **2006**, *89*, art no. 253104.
- (18) Krahne, R.; Morello, G.; Figuerola, A.; George, C.; Manna, L. *Phys. Rep.* **2011**, *501*, 75–221.
- (19) Deka, S.; Genovese, A.; Yang, Z.; Miszta, K.; Bertoni, G.; Krahne, R.; Giannini, C.; Manna, L. *J. Am. Chem. Soc.* **2010**, *132*, 8912–8914.
- (20) Choi, J.; Kang, N.; Yang, H. Y.; Kim, H. J.; Son, S. U. *Chem. Mater.* **2010**, *22*, 3586–3588.
- (21) Zhao, Y. X.; Pan, H. C.; Lou, Y. B.; Qiu, X. F.; Zhu, J. J.; Burda, C. *J. Am. Chem. Soc.* **2009**, *131*, 4253–4261.
- (22) Sadtler, B.; Demchenko, D. O.; Zheng, H.; Hughes, S. M.; Merkle, M. G.; Dahmen, U.; Wang, L. W.; Alivisatos, A. P. *J. Am. Chem. Soc.* **2009**, *131*, 5285–5293.
- (23) Riha, S. C.; Johnson, D. C.; Prieto, A. L. *J. Am. Chem. Soc.* **2010**, *133*, 1383–1390.
- (24) Luther, J. M.; Jain, P. K.; Ewers, T.; Alivisatos, A. P. *Nat. Mater.* **2011**, *10*, 361–366.
- (25) Hermann, A. M.; Fabick, L. *J. Cryst. Growth* **1983**, *61*, 3.
- (26) Yumashev, K. V. *J. Appl. Spectrosc.* **2000**, *67*, 275–281.
- (27) Gurin, V. S.; Prokopenko, V. B.; Alexeenko, A. A.; Wang, S. X.; Yumashev, K. V.; Prokoshin, P. V. *Int. J. Inorg. Mater.* **2001**, *3*, 493–496.
- (28) Hessel, C. M.; Pattani, V. P.; Rasch, M.; Panthani, M. G.; Koo, B.; Tunnell, J. W.; Korgel, B. A. *Nano Lett.* **2011**, *11*, 2560–2566.
- (29) Additional details on materials and methods are available in the Supporting Information.
- (30) Bohren, C. F.; Huffman, D. R. *Absorption and Scattering of Light by Small Particles*; Wiley: New York, 1998.
- (31) Mansour, B. A.; Demian, S. E.; Zayed, H. A. *J. Mater. Sci.: Mater. Electron.* **1992**, *3*, 249–252.
- (32) Kreibig, U.; Vollmer, M. *Optical Properties of Noble Metal Clusters*; Springer: New York, 1995.
- (33) Maier, S. A. *Plasmonics: Fundamentals and Applications*; Springer: New York, 2007.